ScienceDirect

IFAC-PapersOnLine 48-1 (2015) 421–426

Multi-phase and Multi-component CFD Analysis of a Load – Sensing Proportional Control Valve

E. Bigliardi*, M. Francia*, M. Milani*, L. Montorsi*, F. Paltrinieri*, M. Stefani*

** Department of Sciences and Methods for Engineering, University of Modena and Reggio Emilia, Reggio Emilia, Italy, (e-mail: massimo.milani@unimore.it)*

Abstract: The paper analyzes the flow through a directional control valve for load –sensing application by means of a multi-phase and multi-component CFD approach. Numerical modeling includes both cavitation and aeration; in particular, the Rayleigh-Plesset equation and the inertia controlled growth model for bubble formation are adopted. The effects of gas release and vapor formation as well as turbulence on the main valve metering characteristics are investigated. The results show a remarkable influence of the aeration phenomena on the recirculating zones downstream of the metering area and thus on the cavitation onset region. The flow forces on the valve spool are also analyzed and different calculation approaches are compared.

Keywords: CFD, cavitation, aeration, control valve

1. INTRODUCTION

Numerical analysis is gaining an important role in the design of hydraulic components and systems. In particular, multidimensional simulation is increasingly applied to the investigation of the fluid dynamics behavior of hydraulic component in order to broaden and complete the experimental campaigns. Moreover, the human and computational resources to be involved in the numerical analysis are now not only acceptable, but also advantageous, due to the continuous development of computational platforms and CFD tools.

In literature, many examples are available concerning the advantages gained by using the numerical analysis. Among them, several applications on the study of hydraulic valves can be pointed out; for instance, in Yang (2004 and 2005) the CFD analysis was used to study the flow field and the flow-induced forces in hydraulic valves, as well as in Borghi et al. (2000, 2005 and 2005) and in Del Vescovo et al (2003) and in Franzoni et al. (2008), theoretical approaches and experimental investigations have been compared to CFD predictions for the hydraulic valves design and optimization.

In this paper the metering characteristics of a closed center load – sensing proportional control valve are investigated using the multi-phase multi-component numerical simulation. The CFD tool is used to simulate the effects of different operating conditions on the valve flow characteristics. In particular, several opening displacements and pressure drops are analysed and the onset regions for aeration and cavitation are addressed.

The hydraulic valve performance is evaluated in terms of overall discharge coefficient, efflux angle, flow forces and pressure and velocity distributions in the critical region.

2. CONTROL VALVE GEOMETRY

The control valve under study (see Figure 1) is the main metering part of an electro-hydraulic load-sensing proportional valve, usually adopted in multi-slice blocks to control parallel actuations of industrial, agricultural and earthmoving applications.

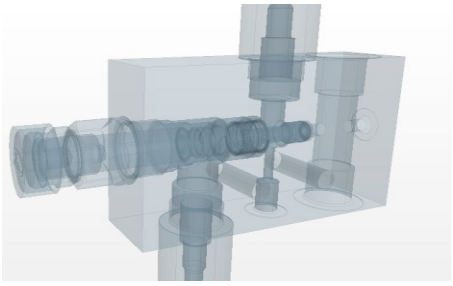

Figure 1. The analysed geometry.

As well known, the application of the load-sensing concept to hydraulic circuit enables efficient management of the hydraulic power delivered to actuators and improves the overall system efficiency.In its simpler design, the proportional control valve for load-sensing applications is intended to directly react to a pressure signal (coming from the actuator) in order to maintain as constant as possible the pressure drop across their metering edges. This action is normally influenced by a local pressure compensator which could have either a single or a double stage configuration, and is usually placed upstream or downstream the control valve center. Therefore, for a given operating position of the control valve spool, and for the flow-rate across the efflux area of metering orifices the pressure drop can be maintained constant independently by the actuator work-load.

10.1016/j.ifacol.2015.05.114

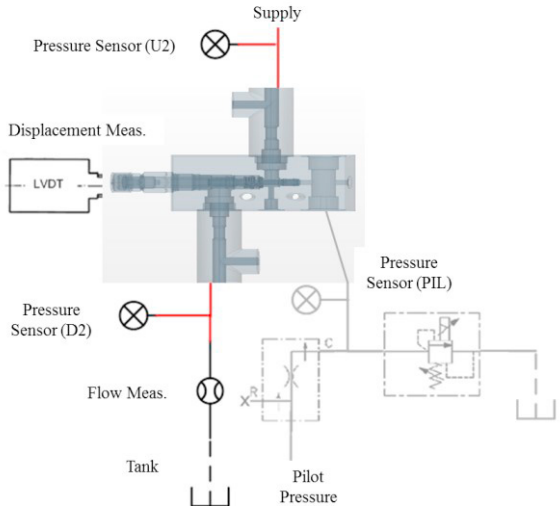

Figure 2. Layout of the test rig.

The Figure 2 shows the schematic of the layout of the test rig used in the Manufacturer's R&D Department for measuring the flow rates and pressure drops for the load-sensing proportional control valve studied here. In particular, the valve is designed for operational field limits up to 150 l/min as maximum flow-rate and up to 350 bar as maximum pressure.

Figures 3 and 4 detail the metering characteristics of the proportional control valve central edge, as determined for an operating condition involving the flow-rate addressed to the control block for a varying pressure drop between the inlet and outlet ports (i.e. D2 and U2 respectively).

More in details, Figure 3 highlights the flow-rate metering curve, as obtained by varying the pressure drop across the valve for a constant spool displacement. Due the slow transient condition the curve is practically symmetrical with respect to the mid point of the time history.

3. NUMERICAL APPROACH

The CFD analysis of the load sensing proportional control valve is carried out by means of the computational fluid dynamics code STAR-CCM+, licensed by CD-Adapco. Bounded central differencing is used for the discretization of the momentum, second-order scheme for subgrid kinetic energy, and the mixture fraction. The conservation equations for mass, momentum, and energy are solved simultaneously using a pseudo-time-marching approach The second-order implicit method is used for time integration scheme.

The cavitation model available in the code and used in this work is based on the Rayleigh-Plesset equation and uses the inertia controlled growth model for bubble formation. The mutli-component cavitation bubble growth rate is estimated using the inertia controlled growth model described in Sauer (2000):

$$\left(\frac{DR}{Dt}\right)^2 = \frac{2}{3}\left(\frac{p_{sat,m} - p_\infty}{\rho_l}\right) \qquad (1)$$

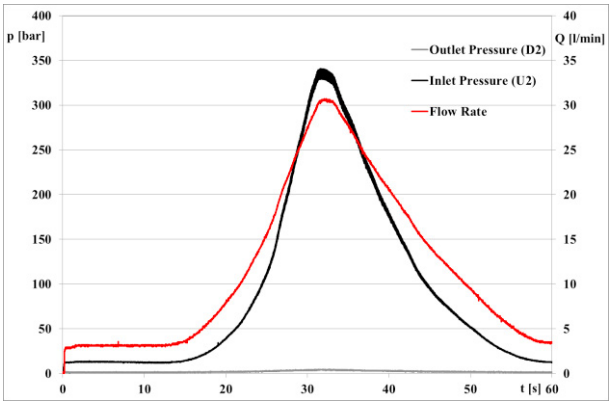

Figure 3. Measured flow parameters for 0.2 mm displacement.

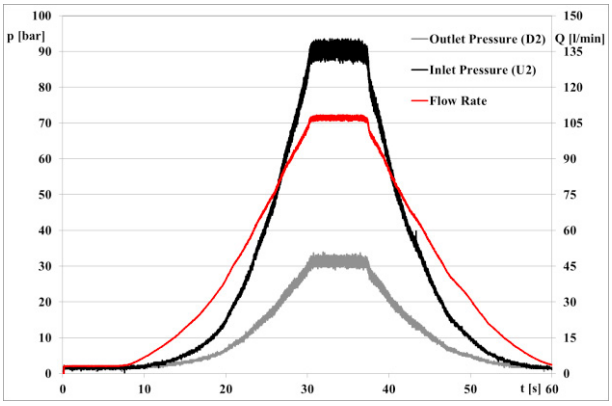

Figure 4. Measured flow parameters for 1.5 mm displacement.

where the mixture saturation pressure is defined as follows:

$$p_{sat,m} = \sum_i^{N_c} X_{i,l,s} p^*_{sat,i} \qquad (2)$$

This expression is Raoult's Law, with $p^*_{sat,i}$ indicating the saturation pressure of the pure component. The interfacial molar fraction of the liquid components is approximately their value in the bulk, so $X_{i,l,s} \approx X_{i,l,\infty}$.

In Eqn. (1), $p_{sat,m}$ is the saturation pressure corresponding to the temperature at the bubble surface, p_∞ is the pressure of the surrounding liquid and is the liquid density. Eqn. (1) is a simplification of the more general Rayleigh-Plesset equation which takes into account the inertia, viscous, and surface tension effects:

$$R\frac{d^2R}{dt^2} + \frac{3}{2}\left(\frac{dR}{dt}\right)^2 = \frac{p_{sat} - p_\infty}{\rho_l} - \frac{2\sigma}{\rho_l R} - 4\frac{\mu_l}{\rho_l R}\frac{dR}{dt} \qquad (3)$$

μ_l is the liquid viscosity and σ is the surface tension coefficient. Research results suggest that for most practical applications, it is not necessary to account for the viscous and surface tension effects as described in Brennen (1995).

This multicomponent formulation neglects the effect of other gases that are present in the bubbles (for example, as a consequence of gas dissociation) and which have their own partial pressure in the bubble. Homogeneous models compute only the pressure of the entire phase mixture, rather than computing a pressure for each individual phase.

The deabsorption of liquid air dissolved into the operating fluid is simulated using a numerical approach similar to cavitation and accounting for the proper saturation pressure.

The CFD domain, see Figure 5, used in the simulations includes the metering edges of the control valve, the inlet duct and the outlet region up to the central volume where usually a local pressure compensator is positioned. The corresponding mesh is created using an unstructured polyhedral grid paying particular care to the metering areas. Local refinements are used to obtain a large number of cells in the critical sections and at small opening positions. Moreover, wall cell layers are employed in order to have the proper wall cell height accordingly to the adopted turbulence model. The average mesh resolution is set to 0.1 mm corresponding to an overall cell number equal to 3 million elements. Figure 6 shows the mesh of the entire CFD domain for a mid range opening position as well as zoomed views of a the metering edge. In the numerical analysis, several spool positions are considered in order to simulate different operating conditions of the control valve. In particular four spool displacements are investigated.

Table 1 details all the operating conditions used in the analysis. For all simulated cases, the Reynolds number resulted in the fully turbulent region. Therefore, in the simulations carried out for the present work the turbulence is modeled by means of the two zonal version of the k-ω model, known as the shear stress transport model. Furthermore, careful attention is paid in order to comply with the requirements on the y^+ values for the turbulence model adopted.

Table 1. Spool displacements and operating conditions used in the simulations.

Spool Displacement [mm]	**Flow Rate [l/min]**				
0.2	5	10	15	20	30
0.5	10	20	30	50	70
1.0	20	40	60	80	100
1.5	20	40	60	80	100

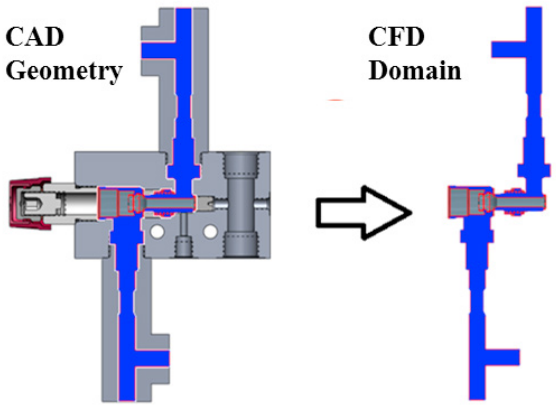

Figure 5. The geometry of the control valve included in the CFD domain.

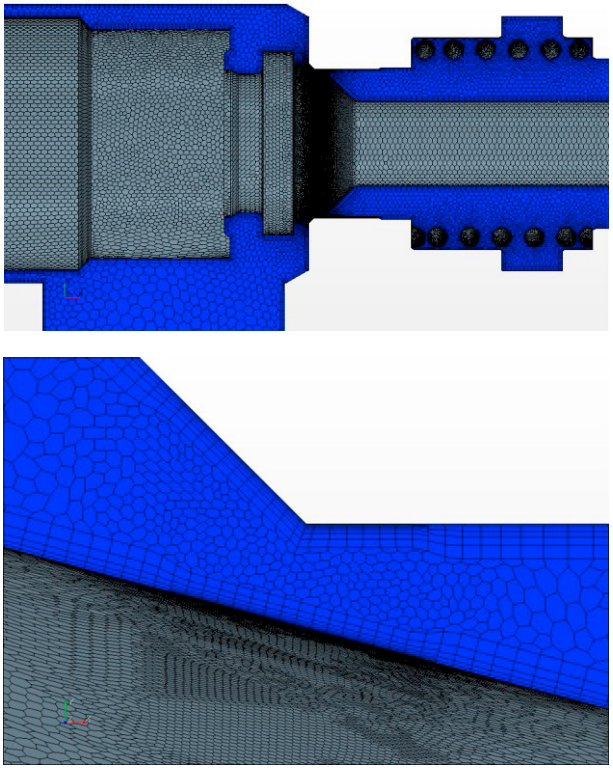

Figure 6. a) The CFD grid for the metering section of the proportional control valve; b) detail of the mesh in the metering area.

4. RESULTS

The results of the numerical analysis of the proportional control valve are discussed in terms of discharge coefficients, pressure total drop, flow acceleration angles and flow forces. In particular the onset regions for aerating and cavitating phenomena are highlighted.

Figure 7 depicts the comparison between the measured and calculated pressure drop across the valve at varying flow rate and for the different spool displacements. The experimental curves represent the maximum and minimum measured value for that operating condition, in order to

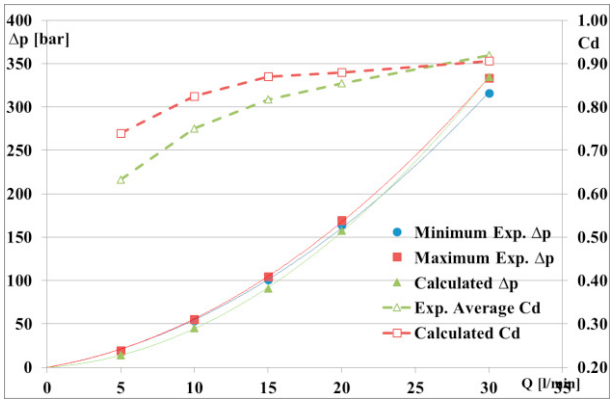

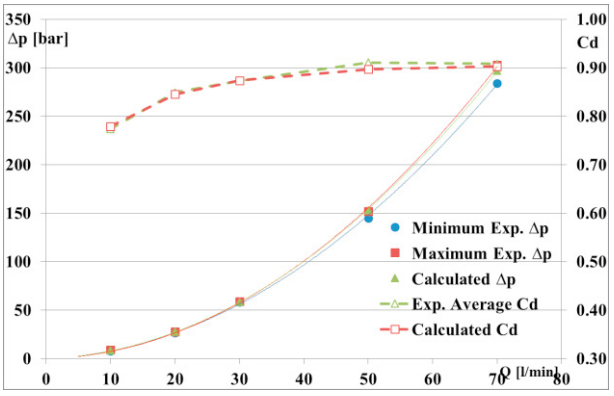

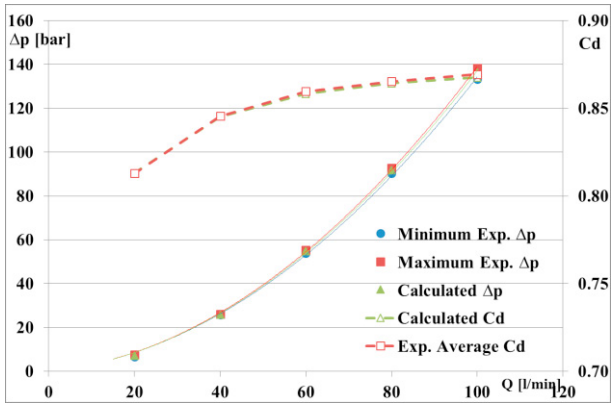

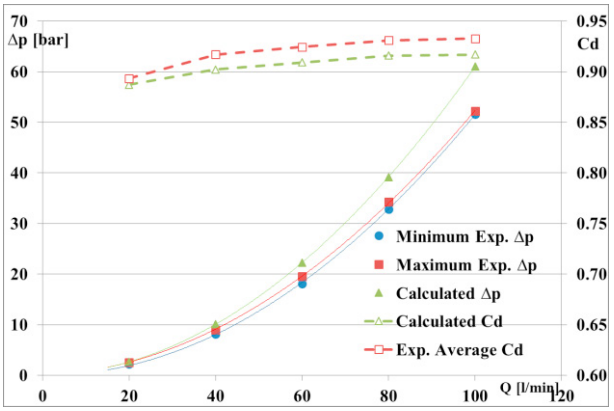

Figure 7. Comparison between Experimental and calculated values for the total valve pressure drop and the discharge coefficient (spool displacement equal to a) 0.2 mm, b) 0.5 mm, c) 1.0 mm and d) 1.5 mm).

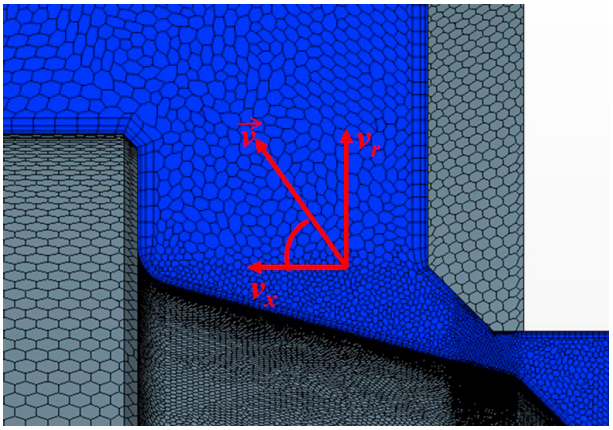

Figure 8. Reference cylindrical coordinate system for the efflux angle calculation.

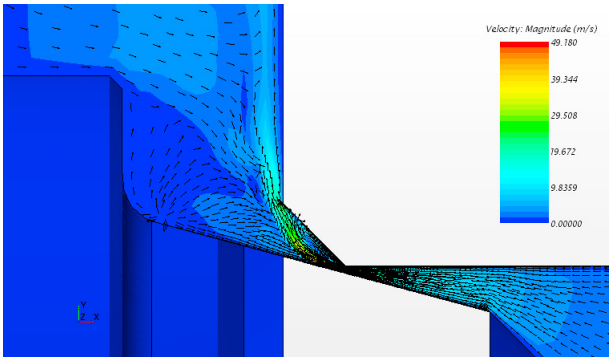

Figure 9. Velocity flow field and vectors used for the calculating the efflux angle.

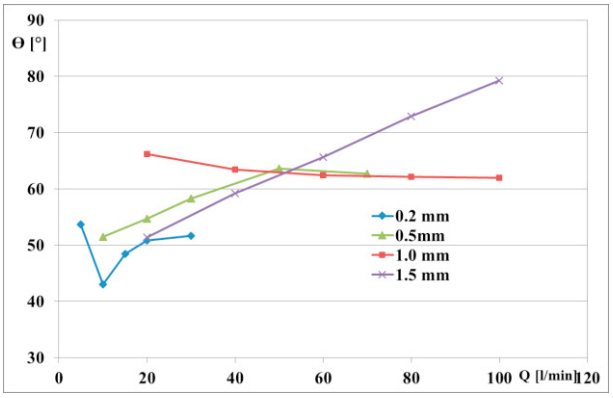

Figure 10. Calculated efflux angle for the different spool displacements.

address the variation achieved by the employed sensors. In the simulations, the outlet pressure is assumed as a constant boundary condition, while the inlet pressure is calculated because of the fluid – dynamics losses through the metering edge. Calculated values lie in the tolerance range of the measurements carried out; thus the numerical discharge coefficients are in good agreement with the experimental ones. It can be noticed that the permeability of the analysed valve results to be remarkably high; in fact, the values of the Cd are in the range between 0.8 and 0.9 and decrease below 0.7 only at low flow rate and for the smallest spool displacement.

Figure 8 shows the reference cylindrical coordinate system employed for calculating the efflux angle. The reference system is centred on the spool axis and the axial and radial components are used to estimate the flow acceleration angles for the simulated cases, see Eqn. (4). Figure 9 depicts the velocity vector distribution in the metering area; an ad-hoc function is implemented in the CFD code to estimate the efflux angle during the computation.

$$\theta = \arctan\left(\frac{v_r}{v_x}\right) \qquad (4)$$

In Figure 10 the flow acceleration angles are plotted for the different simulated operating conditions. The efflux angle result to vary between 40 and 80 degree and it is remarkably influenced by both the flow rate and the spool displacement. The former has more evident effects in case of high spool displacement. As a common trend, the efflux angle tends to increase while the flow rate increases, with the exception of the aperture equal to 1.0 mm. In this operating condition the efflux angle result more constant as the flow rate rises. Likely, below the 1.0 mm opening the flow is still strongly influenced by the geometry of the metering edge, while above that value the effect of the compensator becomes more relevant. As far as the flow forces are concerned, Figure 11 shows the comparison between the calculated values (solid line) and the experimental estimation (dashed line). The latter values are determined by evaluating the pressure forces acting on the inlet and outlet surfaces at the opposite side of the spool (see Figure xx). Thus, the flow forces are estimated by multiplying the total pressure drop across the valve and the relating surface, see Eqn. 5.

$$F_{fl,\exp} = \Delta p \cdot \pi \cdot \left(r_1^2 - r_2^2\right) \qquad (5)$$

From Figure 11 a) it is possible to outline that the experimental estimation of the flow forces tends to underestimate the total forces acting on the spool and influencing the valve actuation. Even though this result could be explained by observing that the experimental values neglect the effects of the shear stresses exerting by the fluid on the spool surface as a consequence of the viscosity, on different geometries of the valve metering edge the numerical flow forces result to be lower that the experimental calculations. This behaviour is observed in particular for the larger spool displacement where the pressure drop does not occur entirely in the metering area but the pressure losses are significant also before the throat area. In fact, in this condition that area becomes comparable with the section area within the spool. Thus the total pressure drop acts on a smaller surface than the one assumed in Eqn. 5 which tends to overestimate the total flow force, see Figure 11 b).

Finally, the aeration and cavitation regions in the metering area are investigated. From Figure 12, it is possible to notice that the pressure reduces far below the saturation pressure of both the air dissolved in the operating and the oil vapour. Figure 13 shows large aeration regions downstream of the

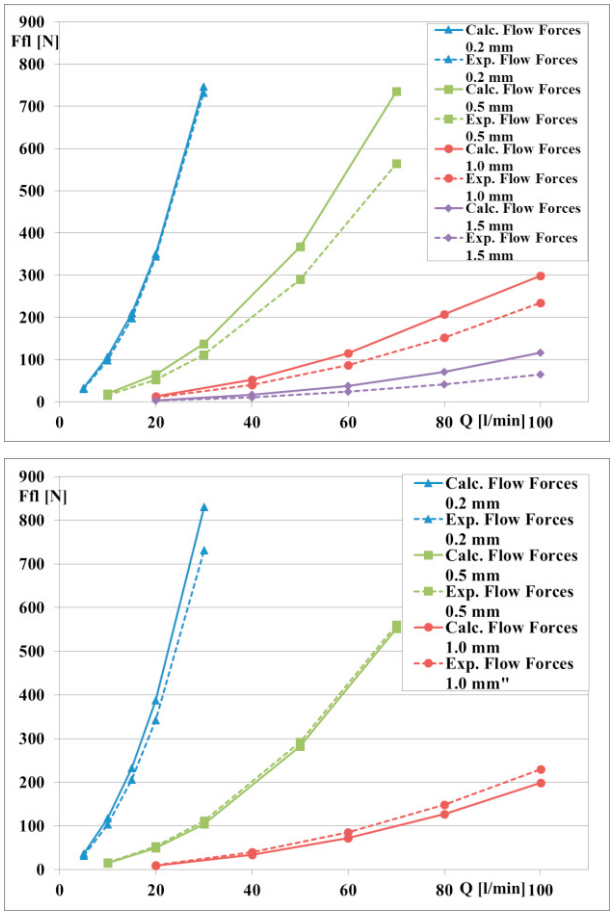

Figure 11. Comparison between Experimental and calculated flow forces for different spool displacements (a) baseline geometry and b) different compensator diameter).

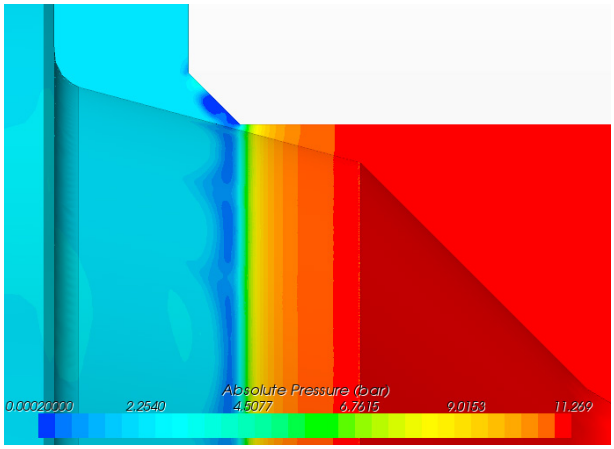

Figure 12. Pressure distribution in the metering area (spool displacement equal to 0.2 and flow rate equal to 5 l/min).

metering edge and on the outer radius. This region is where vortices appear due to the turbulent flow that are caused by the pressure gradient and the geometry, see Figure 9. Nevertheless, the onset areas for aeration and cavitation are far smaller than the recirculating zones and low-pressure regions. This behaviour is explained by investigating the amount of air dissolved in the oil. Figure 14 remarks that in the region downstream of the aeration onset area the

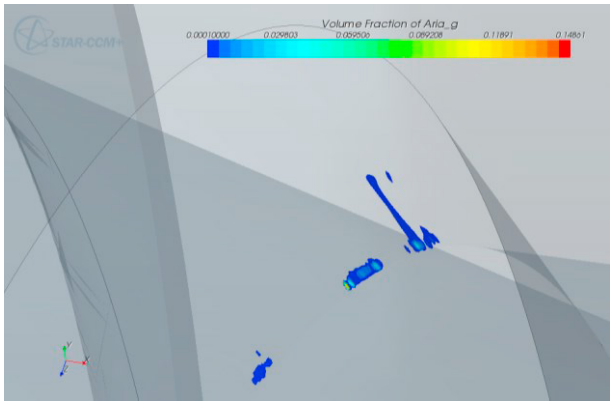

a)

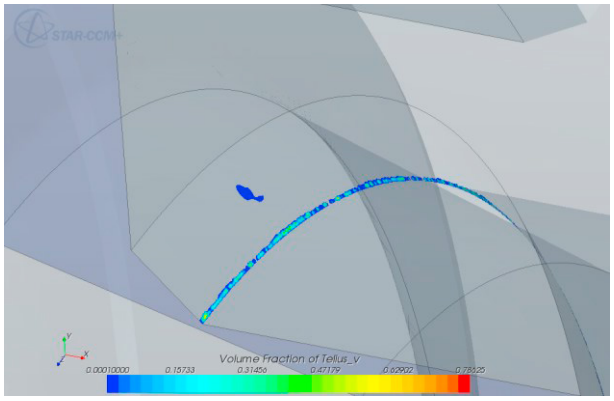

b)

Figure 13. a) Released gaseous air and b) oil vapour formation in the metering area (spool displacement equal to 0.2 and flow rate equal to 5 l/min).

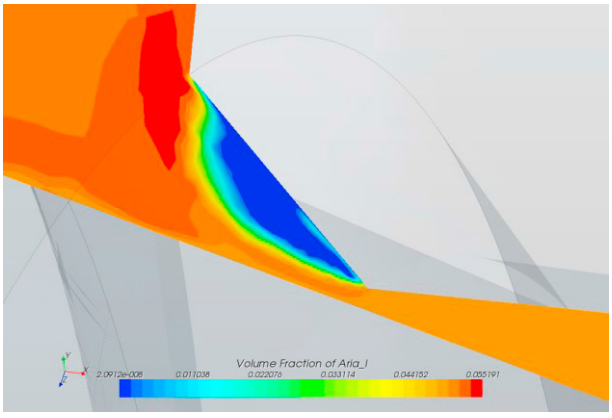

Figure 14. Zoomed view of the dissolved air distribution in the metering area (spool displacement equal to 0.2 and flow rate equal to 5 l/min).

remaining dissolved air in the oil is rather small and this prevents further formation of gaseous air. In fact, when the oil having still a significant content of dissolved air mixes with the degasified oil, the pressure has already increased above the air saturation value.

5. CONCLUSION

A multi-phase multi-component CFD approach has been applied to investigate the flow through the metering edge of a load – sensing proportional control valve. The numerical simulation included models for cavitation, gas absorption and release and turbulence. Different operating conditions as well as spool displacements were analysed in terms of overall discharge coefficient, efflux angle, flow forces and pressure and velocity distributions in the critical region.

The numerical results demonstrated to be in good agreement with the experimental measurements in terms of total pressure drop across the valve as well as in terms of discharge coefficients.

Significant differences were outlined between the numerical value and the experimental estimation when evaluating the flow forces. In particular, the latter method for determining the forces exerted by the fluid on the spool surfaces neglects the effects of the shear stresses on the spool wall. Moreover, the assumption of the total valve pressure drop acting on the entire inlet and outlet surfaces on the spool resulted to be limiting, in particular for the large apertures and flow rates. In these cases, the experimental estimation proved the underestimate the total flow forces.

Finally, the onset areas for aeration and cavitation were investigated. The simulation proved that these regions are located downstream of the metering edge on the outer radius where flow recirculation takes place. Nevertheless, the aeration region resulted to be smaller than the low-pressure zone due to a degasification effect of the onset area, which released almost the entire content of air dissolved in the operating fluid thus preventing further aeration even though the pressure remained below the saturation value.

REFERENCES

Borghi, M., Milani, M., Paoluzzi, R. (2000) Stationary axial flow force analysis on compensated spool valves. *International Journal of Fluid Power* 1 No. 1 p.p. 17-25.

Borghi, M., Milani, M., Paltrinieri, F. (2004). The Influence of the Notch Shape and Number on Proportional Directional Control Valves Metering Characteristics. *SAE Paper* 2004-01-2619.

Borghi, M., Milani, M., Paoluzzi, R. (2005). Influence of Notch Shape and Number on the Metering Characteristics of Hydraulic Spool Valves. *International Journal of Fluid Power*. ISSN 1439-9776 - Vol. 6, N. 2 - pp. 5-18.

Brennen, C.E. (1995) Cavitation and Bubble Dynamics, *Oxford University Press*.

Del Vescovo, G., Lippolis, A. (2003). Three Dimensional analysis of flow forces on directional control valves. *International Journal of Fluid Power*. Vol.4 Number 2.

Franzoni, F., Milani, M., Montorsi, L., (2008) Cavitating Flows in Hydraulic Multidimensional CFD Analysis, *SAE Paper* 2008-01-678.

Yang, R. (2004) Improving Spool Valve Operating Effort Using CFD, *SAE Paper* 2004-01-2620.

Yang, R. (2005) Predicting Hydraulic Valve Pressure Drop Using CFD, *SAE Paper* 2005-01-3635.

Sauer, J. (2002) Instationaer kavitierende Stroemungen - Ein neues Modell, basierend auf Front Capturing VOF und Blasendynamik, Dissertation, *Universitaet Kalrsruhe*.